A review of methods on buildability quantification of extrusion-based 3D concrete printing From analytical modelling to numerical simulation

Chang, Ze; Chen, Yu; Schlangen, Erik; Šavija, Branko

DOI
10.1016/j.dibe.2023.100241

Publication date
2023

Document Version
Final published version

Published in
Developments in the Built Environment

Developments in the Built Environment 16 (2023) 100241

Contents lists available at ScienceDirect

Developments in the Built Environment

journal homepage: www.sciencedirect.com/journal/developments-in-the-built-environment

A review of methods on buildability quantification of extrusion-based 3D concrete printing: From analytical modelling to numerical simulation

Ze Chang *, Yu Chen, Erik Schlangen, Branko Šavija

Microlab, Faculty of Civil Engineering and Geosciences, Delft University of Technology, Delft, the Netherlands

ARTICLE INFO

Keywords:
3D concrete printing
Numerical analysis
Buildability quantification
Printing process

ABSTRACT

Herein, different kinds of methods for buildability quantification of 3D concrete printing are reviewed, including experimental approaches, analytical modelling, and numerical simulations. A brief introduction on printing process is first given. This discusses the material properties in different stages. Material printability, which encompasses pumpability, extrudability and buildability, is then discussed. Subsequently, a brief review of the experimental and analytical models for buildability quantification is presented and they're discussed. An overview on the numerical tools for 3DCP is then given. These numerical models can quantify structural buildability and optimize the printing parameters, therefore, providing a more economical solution for buildability quantification. In the end, a summary and discussion on the limitations of numerical tools for buildability quantification are provided, as well as recommendations for their improvement.

1. Introduction

The construction industry serves as a cornerstone of global economy, contributing 6% to GDP and bringing in close to $10 trillion annually (Gerbert et al., 2016; de Soto et al., 2018; Pang et al., 2022a). Despite this, the construction technique remains low-tech, with the majority of construction projects being executed using manual labour (Harty, 2008). Besides, the increase in the number of construction projects results in a heavy burden on the environment (Bonoli et al., 2021). According to the estimation of the United Nations, the global population will rise to around 10.9 billion by 2100. The dramatic growth will result in a significant burden on living and housing (Economic and Division, 1999).

Considering the great burden of conventional construction methods on sustainability and productivity (Wangler et al., 2019; Pang et al., 2022b), it is essential to explore high-efficiency construction strategies. An advanced technology, i.e., 3D concrete printing (3DCP), has been proposed to replace traditional construction techniques with a lower labour-and-resource cost. Buswell et al. (2018) reviewed the number of implemented projects by means of additive manufacturing techniques, as shown in Fig. 1. Clearly, this advanced manufacturing technology generates a growing interest in academic and construction sectors. The projects range from building elements to entire structures, including a cycling bridge in the Netherlands (Salet et al., 2018), houses in China (He et al., 2020), the USA and the Middle East (Asprone et al., 2018; Siddika et al., 2020; Pessoa et al., 2021). In contrast to conventional construction methods, 3DCP can create complex geometries without formwork, thereby resulting in a reduced cost with respect to formwork materials.

Although 3D concrete printing shows potential, full adoption in the construction sector is still far away due to the lack of knowledge regarding material properties and structural behaviours in the fresh state. To understand the material printability, lots of studies have been conducted from different aspects, which include material mixing, pumping, extrusion, building-up, curing, and durability (Dey et al., 2022; Ma et al., 2022; Batikha et al., 2022). In order to provide a common platform to discuss these novel ideas and research findings, three RILEM international conferences on the topic of 3DCP were held in Zurich in 2018 (Wangler and Flatt, 2018), Eindhoven in 2020 (Bos et al., 2020), and Loughborough in 2022 (Buswell et al., 2022).

Herein, a review of structural behaviour of printable concrete in fresh state is provided. This work first summarizes the basic principles of the printing process, consisting of pumping, extrusion and build-up stages. Subsequently, strategies for buildability quantification are reviewed, including experiments, analytical and numerical models. In the end, some limitations of analytical and numerical methods are discussed, and research gaps are identified.

* Corresponding author.
E-mail addresses: z.chang-1@tudelft.nl (Z. Chang), Y.Chen-6@tudelft.nl (Y. Chen), Erik.Schlangen@tudelft.nl (E. Schlangen), B.Savija@tudelft.nl (B. Šavija).

https://doi.org/10.1016/j.dibe.2023.100241
Received 22 July 2023; Received in revised form 25 September 2023; Accepted 28 September 2023
Available online 1 October 2023

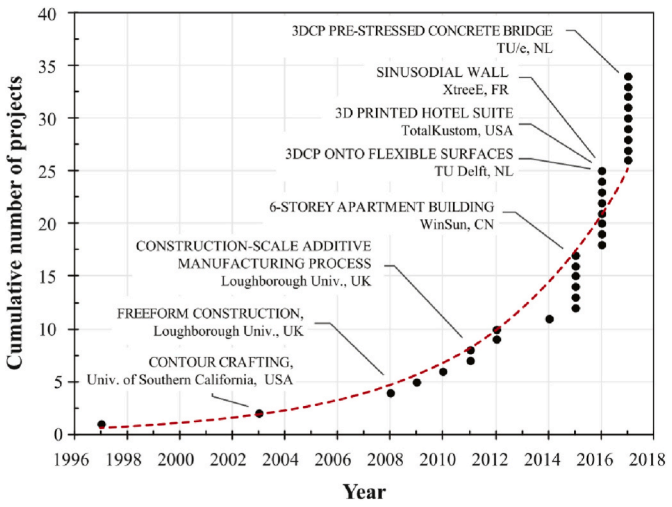

Fig. 1. The increase in number of large-scale concrete 3D printed projects since 1997 (Buswell et al., 2018).

2. Overview of printing stages of 3DCP

The 3DCP process contains at least three stages: a) the pumping stage from pump to nozzle (i.e., the print head) through a pipe or a hose; b) the deposition process through the nozzle; and c) the build-up stage (Vallurupalli et al., 2021; Nerella and Mechtcherine, 2019). In general, three criteria, namely pumpability (Tay et al., 2019; Zhang et al., 2019), extrudability (Ting et al., 2022; Zhi et al., 2022) and buildability (Joh et al., 2020; Nerella et al., 2020; Panda et al., 2019a), are used to describe the material printability in different stages, as described in Fig. 2. Pumpability ensures that printable material can be transferred within pipe without blockage, which requires the material to be flowable. In this stage, the printable materials behavor like the non-Newtonian fluid. Therefore, the rheology and fluid mechanics are generally used to quantify the material pumpability and extrusion ability. After that, the material will be extruded from the print head. The geometry of the nozzle may affect material properties (Roussel, 2006, 2018). This is followed by the structural build-up stage, which requires that the extruded material has sufficient stiffness and strength to sustain its geometry under the loading from itself and subsequent printing layers. Thus, the solid mechanics, which is used for the simulation of solid materials, is commonly used in this stage. There should be a balance between pumpability and buildability (Tay et al., 2019): the former requires the cementitious material to exhibit followability, where it can easily conform and flow, while the latter demands the extruded material to demonstrate shape retainability, where it can maintain its extruded shape and structure.

To assess the printability of cementitious materials, numerical and analytical methods have been proposed over the past several years as alternatives to experiments. Understanding material behaviour during printing process is crucial for mix design and printability assessment.

2.1. Pumping stage

The pumping stage refers to the process during which the cementitious material is conveyed from pump to nozzle. In general, pumpability of cementitious materials can be measured by laboratory testing. To set the optimal parameters for pumping process, a full understanding on the relationship between material pressure and flow rate is required (Feys, 2019; Choi et al., 2013).

Printable cementitious materials are often assumed to behave as Bingham fluids. The traditional Buckingham-Reiner equation is often used to compute the pumping pressure for complex suspensions. However, this equation may overestimate the pumping pressure around 2–5 times (Jo et al., 2012; De Schutter and Feys, 2016) since it does not consider the impact of shear-induced cement particles and segregation and water transfer. The pipe parameters (i.e., length and radius), pump pressure and particle size of printable material codetermine the pumpability during the pumping process (Vallurupalli et al., 2021). Fig. 3 describes the distribution of shear stress and material flow behaviour. Since the cementitious materials for 3DCP are not homogeneous, the shear stress may result in movement of large aggregate particles towards the region with a lower shear rate (namely, the centre of transmission pipe). A 'lubrication layer' (LL) with more water forms near the pipe wall, leaving the 'bulk material' in the pipe's centre (Feys et al., 2016a; Mechtcherine et al., 2020a). The LL is exposed to higher shear stress as compared to bulk material. Because of the migration of cement particles, the material within LL undergoes a structural breakdown process, in which shear stress breaks the connections between cement particles built by flocculation and hydration (Feys et al., 2016b; Roussel et al., 2012). Thus, LL has lower material yield stress and viscosity compared to bulk material (Feys et al., 2016a; Choi et al., 2016). To investigate the impact of pipe and material properties on pumping pressure Δp_{tot}, Kaplan et al. (2005) presented two analytical models. These models incorporate a series of printing parameters and material properties, which include flowrate Q_p, shear yield stress τ_0 and plastic viscosity μ, as shown in Eq. (2) and Eq. (3).

$$Q_p = \pi \frac{3\Delta p_{tot}^4 R^4 + 16\tau_0^4 L^4 - 8\tau_0 L R^3 \Delta p_{tot}^3}{24\Delta p_{tot}^3 \mu L} \quad \text{Eq. 1}$$

$$\triangle P = \frac{2L_{pipe}}{R_{pipe}} \left[\frac{Q_p \mu_i}{\pi R_{pipe}^2 k} + \tau_{0,i} \right] \quad \text{Eq. 2}$$

$$\triangle P = \frac{2L_{pipe}}{R_{pipe}} \left[\frac{\frac{Q_p}{\pi R_{pipe}^2 k} - \frac{R_{pipe}}{4\mu}\tau_{0,i} + \frac{R_{pipe}}{3\mu}\tau_0}{1 + \frac{R_{pipe}}{4\mu}\mu_i} \mu_i + \tau_{0,i} \right] \quad \text{Eq. 3}$$

Where L_{pipe} and R_{pipe} refer to the pipe length and radius. The Q_p and τ_0 are the flowrate and shear yield stress. The μ is the plastic viscosity of printbale materiials.

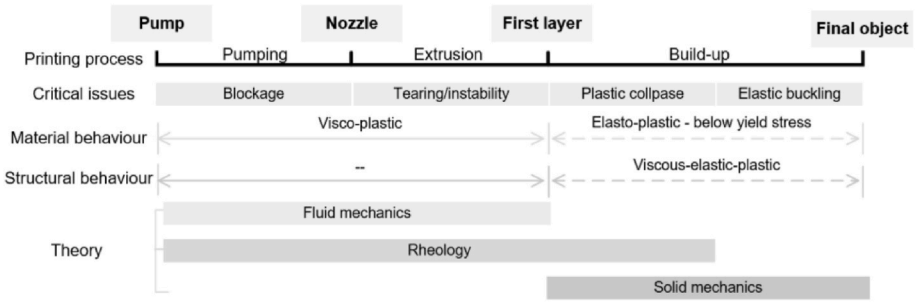

Fig. 2. A schematic diagram of 3DCP at different stages (Chang et al., 2021).

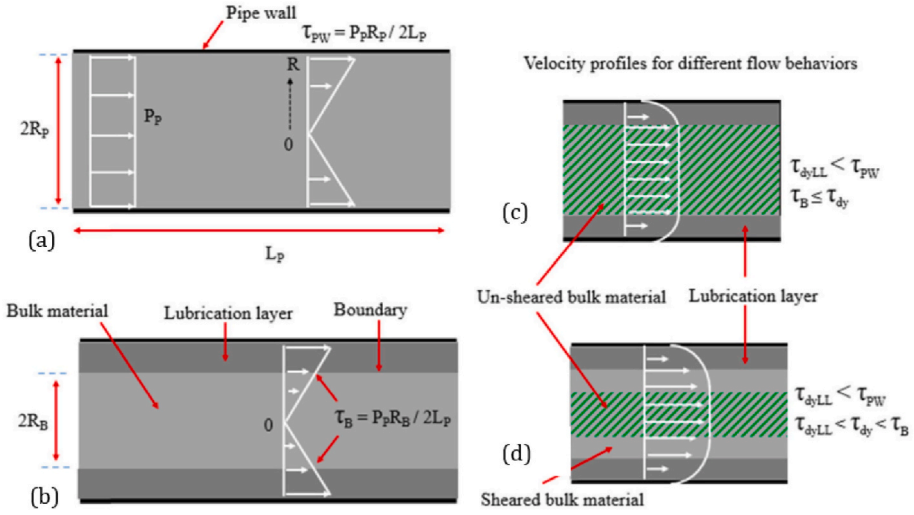

Fig. 3. Pumping processes and flow behaviour in 3DCP (Vallurupalli et al., 2021) (a) pumping process (b) shear stress distribution (c) velocity schematic of material flow during plug flow (d) velocity schematic of material flow during shearing flow.

Besides pipe and material properties, the temperature and air content also affect the pumping pressure. The friction from the transmission pipe may raise the material temperature and cause the material to rapidly dissolve or incorporate air (Feys et al., 2016b; Vosahlik et al., 2018; Das et al., 2020), affecting its rheological properties.

2.2. Extrusion stage

After the pumping stage, the printable material should be extruded from the nozzle. There are two commonly utilized extruder types, namely, a piston or a screw type (Nerella et al., 2019a; Perrot et al., 2018; Mohan et al., 2021; Cao et al., 2022) (Fig. 4). In the piston extrusion, the barrel is filled with printable material, the piston then applies pressure from the pump to push the material out of the nozzle (El Cheikh et al., 2017; Panda et al., 2019b). An Archimedes screw or a similar device is generally used for screw extrusion (Hass and Bos, 2020; Sanjayan et al., 2021), enabling a continuous supply of material to the extruder (Jo et al., 2020).

In the piston extruder, the stress condition of the extruded material depends on the nozzle configuration. According to Roussel (2018), there are two commonly utilized nozzles, as shown in Fig. 5. When a rectangular nozzle is used, the cementitious material is extruded in an unsheared condition. A high static yield stress can be obtained after material deposition. Consequently, the extruded material is stiff and the geometry of printed filament is close to cross-section of the nozzle (Roussel et al., 2020). The second type involves a non-laminar flow from a conical nozzle, and the extruded material is subjected to shear stress because of the transition of cross-section of printhead. In this regime, the competition between gravity and yield stress determines the final shape of the extruded layer.

These two cases also introduce different additional loadings to the printed structure during the extrusion process (Cao et al., 2022). If the thickness of the individual layer is larger than “stand-off distance” (i.e., the distance between print head and previously deposited layers), the printed filament will be locally compressed and deformed until the layer height decreases to that distance. For the rectangular nozzle, the printed filament is generally placed on previously printed structure without compression, given that the stand-off distance is larger than the layer height. In such a case, the next printed segment may ‘drop’ into the printed structure, thereby threatening its stability (Wolfs, 2019), as illustrated in Fig. 6. When it comes to the buildability quantification, this additional load may affect the structural build-up capacity.

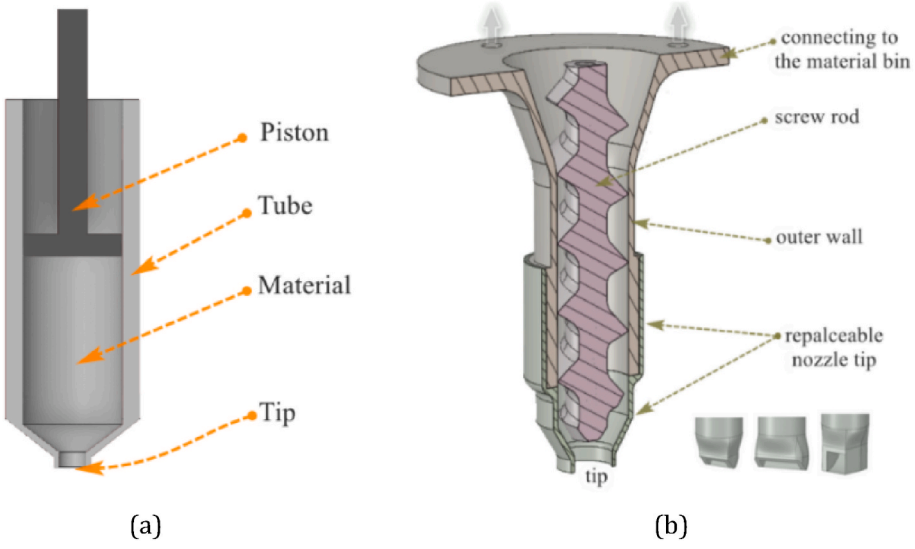

Fig. 4. Two commonly used extruder types in 3DCP (Cao et al., 2022) (a) a piston extruder; (b) a screw-type extruder.

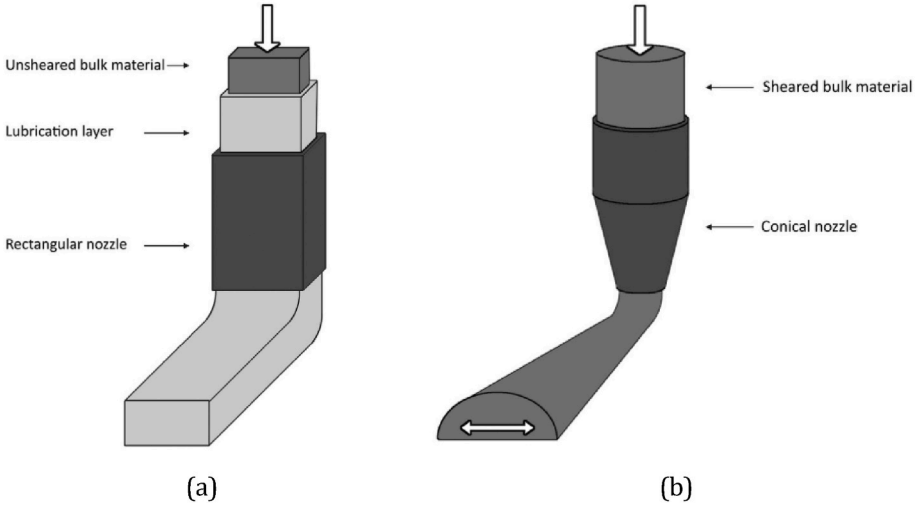

Fig. 5. Two printing cases at the printhead and deposition zone levels (Roussel, 2018) (a) laminar flow from rectangular kind of nozzle (b) non-laminar flow from conical kind of nozzle.

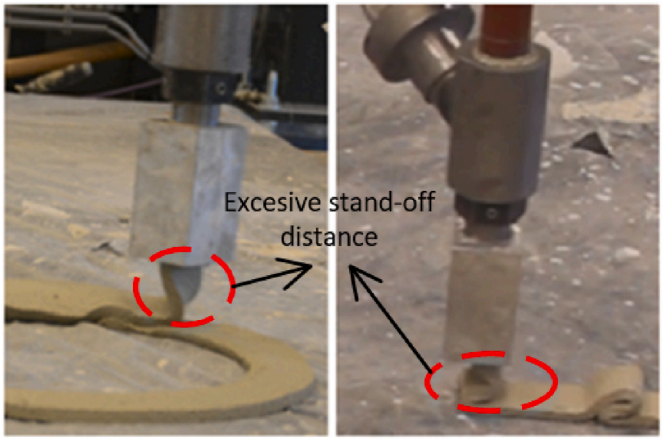

Fig. 6. Illustration of printing problems caused by the excessive standoff distance (Wolfs, 2019).

In order to adjust the height between print head and previous layer, accessories can be installed into the nozzle to monitor the flatness (Wolfs, 2019; Kazemian et al., 2019; Mechtcherine et al., 2020b), layer height, width and stand-off distance. The monitoring signal is sent back to the printer in order to adjust the nozzle height in a real time, as shown in Fig. 7. In that case, the influence of dynamic loading, which is detrimental to structural stability, can be eliminated.

Besides the installation of nozzle accessories, a two-pipe printing strategy has been proposed to ensure good buildability of printable cementitious materials (Tao et al., 2021, 2022a, 2022b; Reiter et al., 2020; Maltese et al., 2007) (as shown in Fig. 8). Unlike the single pipe approach, in which the accelerators are added in the mixing process, in the two-pipe method the accelerator is added into the printed material in the nozzle. This can not only ensure the material stiffness after deposition, but also avoid the high pumping pressure and blockage during the pumping process. Currently, there are two commonly utilized two-pipe systems: dynamic and static mixers. The dynamic mixer refers to the machine with one or more electric motor-driven shafts (Zhang et al., 2012); the static mixer is employed to continuously mix a liquid material, by means of a number of fixed baffles instead of moving components (Thakur et al., 2003). In contrast to the dynamic mixing system, no issues with dead zones occur in the two-pipe pumping system since it uses a static mixer. Additionally, when using a static mixer, significantly higher pumping pressure is required compared to using a dynamic mixer (Rauline et al., 2000). In addition, it should be noted that printable materials with different properties can be mixed using various kinds of static mixers. Further research is required to assess the practicability and their influence on mix homogeneity and required pumping pressure for cementitious-based materials.

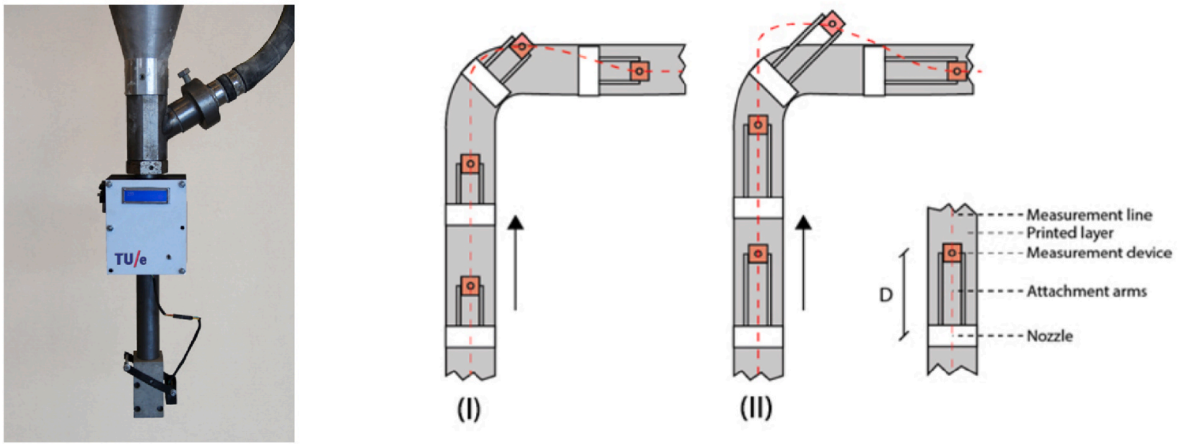

Fig. 7. Nozzle height measuring equipment (left); the position of this device during printing process from the top view (right) (Wolfs, 2019).

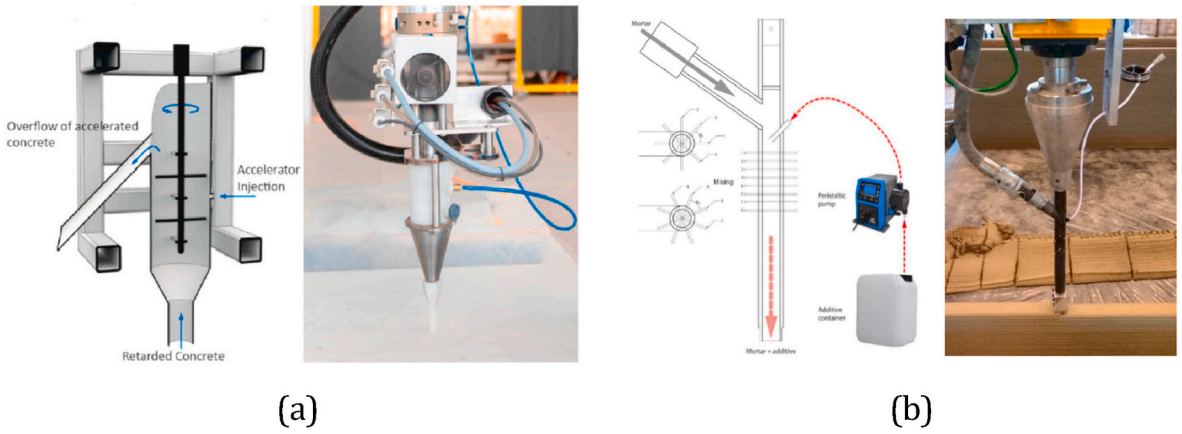

Fig. 8. 3D concrete printing using accelerators added through inline mixing process (a) a mixing reactor for smart dynamic casting that has a pin mixer type tool (left); a mixing reactor for extrusion-based 3D printing which has a pin mixer type tool (right) (Reiter et al., 2020) (b) liquid additive injection equipment. A schematic diagram for this setup (left); a general view of the accelerator injection during printing process (right), taken (Maltese et al., 2007).

2.3. Build-up stage

Extrusion-based concrete printing can create the computer-designed geometry without external support. This can eliminate the need for formwork, thereby decreasing the amount of waste in construction. However, the absence of the formwork during the extrusion process raises the possibility of structural failure after material deposition (Mechtcherine et al., 2020a; Bos et al., 2016; Perrot et al., 2021). During the printing process, gravitational loading from successive printing layers increases. Subject to the gradual incremental loading, the printed structure may fail due to material yielding, structural instability dominant, or a combination of the two. In 3DCP, the material yielding will lead to the structural failure of plastic collapse however, the elastic buckling is used to describe the structural instability. These typical failure modes can be found in Fig. 9.

In general, to prevent structural failure during printing process, both material strength and stiffness of the deposited materials should develop to defend the gradually increasing loading of the printed structure (Reiter et al., 2018; Leal da Silva et al., 2019; Chen et al., 2020; Perrot et al., 2016). This increment of gravitational loading is codetermined by printing speed and material density.

To quantify whether and when the printed structure may fail during printing process, different approaches have been proposed. These methods compare the (minimal) development of material stiffness and strength to the (maximal) printing speed of designed structure. In the following section, a detailed review of the strategies for buildability quantification of 3DCP will be given from the perspectives of experimental investigation, analytical modelling and numerical simulation.

3. Methods for buildability quantification

3.1. Experimental methods

Buildability is a complicated and process-specific feature that is codetermined by material composition and a series of parameters, such as printing velocity and geometry (Nerella et al., 2020; Cui et al., 2022). Le et al. (2012) stated that the most straightforward approach to assess buildability of cementitious materials is through printing trials, in which the critical printed layers (i.e., maximum number of printed layers) can be experimentally measured given a specific printing geometry. Hollow cylinder (Wolfs et al., 2018; Moini et al., 2022), square (Wolfs and Suiker, 2019; Suiker et al., 2020; Suiker, 2018) and wall structures (Suiker, 2018; Wolfs et al., 2019) are most frequently used for buildability quantification. Three typical failure modes mentioned above can be observed through these printing geometries. Although the printing trials can directly reflect the structural build-up capacity, these test procedures are time-and-labour consuming.

In pursuit of more convenient experimental methods, different studies (Joh et al., 2020; Casagrande et al., 2020; Panda and Tan, 2018; De Vlieger et al., 2023) presented the rheological and compression tests

Fig. 9. Typical failure modes during the printing process (a) plastic collapse dominant failure mode (b) elastic buckling dominant failure mode (c) failure mode between elastic buckling and plastic collapse (Ghent, 2020).

(as shown in Fig. 10) for buildability quantification. Through a series of rheological tests, Le et al. (2012) concluded that there is a range (i.e., 0.3–0.9 kPa)of material strength for material printability assessment. This range is highly dependent on the material mix. If lower than this range, i.e., 0.3 kPa, the fresh materials are too wet, and segregation will occur in the pipe-pump-nozzle system. The extruded materials cannot sustain shape due to excessive deformation. If higher than this range, i.e, 0.9 kPa, the cementitious materials are difficult to extrude and be printed continuously. The 'uniaxial compression' test is another method proposed for buildability quantification. For example, Di Carlo (Di Carlo et al., 2013) presented a compression test to quantify the structural buildability of cylinder samples. Kazemian et al. (2017) presented a cylinder stability test for rapid comparative assessment of the impact of mix design on build-up capacity. In these tests, they regard the layers which are placed on the top of one another as compressive loading applied to the specimen. Panda et al. (Panda and Tan, 2018; Panda et al., 2018a; Paul et al., 2018) defined a shape retention parameter to quantify the structural shape stability. They reported that, if the stand-off distance decreases, the dimensional precision of printed structure is compromised (Nerella et al., 2020).

3.2. Analytical models

The experimental method is a reliable approach to test the buildability of cementitious materials; however, this kind of method is time-and-resource consuming. To assess the structural buildability using a more efficient way, some analytical methods were proposed. These analytical models can be divided into two categories: rheological models and solid mechanics models. The major contribution towards rheological models came from Roussel (2018). He explored how a series of material properties, which includes yield stress, elastic modulus, viscosity, and structuration rate, influence the printability (Roussel, 2018). Proposed criteria evaluate the rheological requirements and examine the final geometrical dimensions of a single filament, which include surface cracking and structural instability. To measure the structural build-up rate, Roussel adopted the parameter A_{thix} (Roussel, 2006) and static yield stress σ_0 to predict the material yielding using Eq. (4).

$$\tau_0(t_{rest}) = \sigma_{0,t=0} + A_{thix} t_{rest} \quad \text{Eq. 4}$$

Here, the t_{rest} refers to the resting time after material deposition, and $\sigma_{0,t=0}$ refers to material initial yield stress. It should be pointed that the

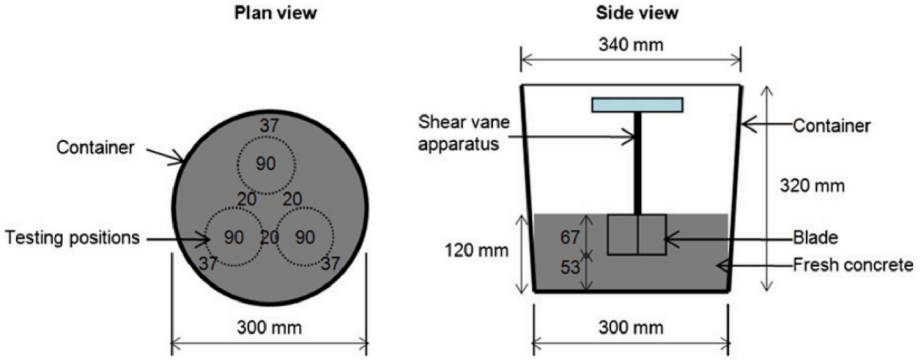

(a)

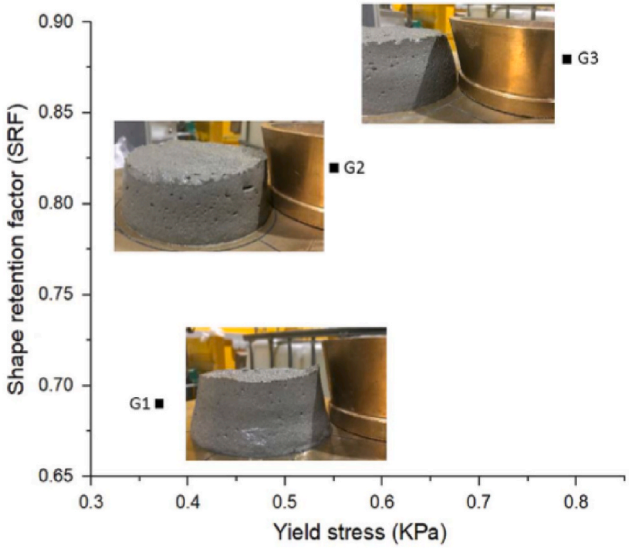

(b)

Fig. 10. Two types of experimental methods for buildability quantification (a) a schematic diagram of shear vane with measuring positions (Le et al., 2012) (b) compression test: relationship between SRF and yield stress of the printable cementitious materials (Panda and Tan, 2018).

sheared extruded material has a lower static yield stress than the unsheared one because of the breakdown of the connection among cement particles, as explained in Section 2.3.2. A_{thix} is the yield stress development due to the structuration and flocculation. According to the time range considered, the material development can be described by a linear or non-linear tendency (Perrot et al., 2015; Lecompte and Perrot, 2017). Further investigations into thixotropy and other rheological properties have been conducted, providing a theoretical basis for research in this field (Zhang et al., 2019; Cardoso et al., 2009; Chen et al., 2018; Jeong et al., 2019; Jayathilakage et al., 2019; Kruger et al., 2019a, 2019b, 2021). These rheological models have been mainly used to characterize the extrusion and pumping processes from the standpoint of material rheology. Kruger et al., 2019c, 2019d, 2019e, 2021 found that re-flocculation of the cement particle network must be taken into account once the printable materials are subjected to high shear stress. They presented a bi-linear model to describe the evolution of material yield stress, which determines the material yielding during the printing process. Two mechanisms (namely, re-flocculation (R_{thix}) and structuration (A_{thix})) are considered with aspects to thixotropic behaviour of printable materials. Fig. 11 depicts the time-dependent yield stress, which is mathematically expressed as:

$$\begin{aligned} &\tau_s(t) = \tau_{D,i} + R_{thix}t \quad \text{for } t \le t_{rf} \\ &\tau_s(t) = \tau_{s,i} + A_{thix}\left(t - t_{rf}\right) \quad \text{for } t > t_{rf} \\ &t_{rf} = \frac{\tau_{s,i} - \tau_{D,i}}{R_{thix}} \end{aligned} \qquad \text{Eq. 5}$$

where $\tau_s(t)$ is the static or the apparent yield stress of the printed material after agitation. $T_{s,I}$ and $\tau_{D,i}$ stand for initial static and dynamic yield stress of printed material, respectively, which can be measured with rheological tests; t_{rf} means the time range in which re-flocculation occurs.

Perrot et al., 2015, 2016 presented a similar analytical model to define the optimal build-up rate considering material yielding. Their model predicts the critical printing height considering instantaneous strength of printed material, as shown in Eq. (6). If the stress in the bottom layer reaches the material strength, plastic collapse is assumed to occur.

$$H_{critical} = \frac{\sqrt{3}\tau_0\left(t_{pr}\right)}{\rho g} \qquad \text{Eq. 6}$$

Here, the t_{pr} refers to the printing time after material deposition. Similarly, Wangler et al. (2016) computed the maximal horizontal printing velocity $V_{\text{r,max}}$, as shown in Eq. (7).

$$V_{r,\max} = \frac{\sqrt{3}LA_{thix}}{\rho g H_{layer}} \qquad \text{Eq. 7}$$

where L refers to the contour length. In contrast to other analytical models, this model studies the impact of structural geometry on the prediction of plastic collapse dominant failure mode since a geometric coefficient is introduced into this equation. However, this parameter is only valid for the typical wall geometry.

However, in addition to plastic collapse, elastic buckling is also important for buildability quantification (Joh et al., 2020; Casagrande et al., 2020). Roussel (2018) presented an analytical model to predict the critical printed height for buckling failure, mathematically described as:

$$H_{c,buck} \simeq \left(\frac{8EI}{\rho g A}\right)^{1/3} \qquad \text{Eq. 8}$$

where E and I refer to the material stiffness and second moment of inertia, and A refers to the horizontal rectangular cross-section area. Then, this model is modified through the consideration of printing geometry. When it comes to wall structure with the I equal to $\delta^3/12$ (δ refers to the width of wall), this equation can be rewritten as:

$$H_{c,buck} \simeq \left(\frac{2E\delta^2}{3\rho g}\right)^{1/3} \qquad \text{Eq. 9}$$

Although other studies also attempted to use similar models to quantify structural build-up (Perrot et al., 2016), the geometry and structural heterogeneity are still difficult to consider (Zhang et al., 2019; Kruger et al., 2019d, 2019f; Panda et al., 2018b; Briffaut et al., 2012; Qian and Kawashima, 2016).

To incorporate the above-mentioned factors, a mechanistic model presented by Suiker (2018) considers a series of parameters, i.e., time-dependent material stiffness and strength, printing velocity, boundary conditions, the structural imperfections and non-uniform gravitational loading. Two failure modes (i.e., elastic buckling and plastic collapse, as shown in Fig. 12), are considered to analyze the build-up performance of a wall structure (Wolfs and Suiker, 2019; Suiker et al., 2020; Suiker, 2018). As explained in Suiker's model (Suiker et al., 2020; Suiker, 2018), the criterion in Eq. (10) can be used to examine whether straight wall structures fail due to elastic buckling or plastic collapse during printing process.

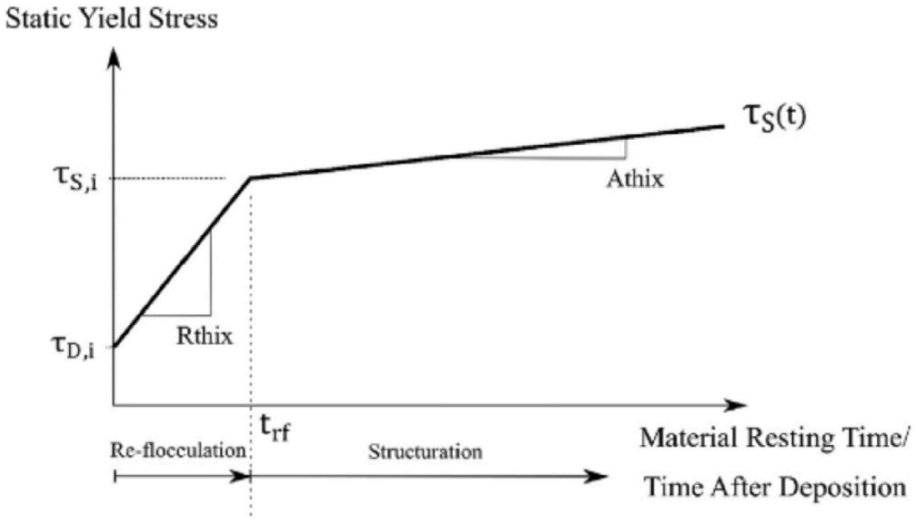

Fig. 11. The development of static yield stress as a function of the concrete age with the consideration of re-flocculation and structuration, the different stages can be mathematically described by Eqs. (2)–(4) (Kruger et al., 2019e).

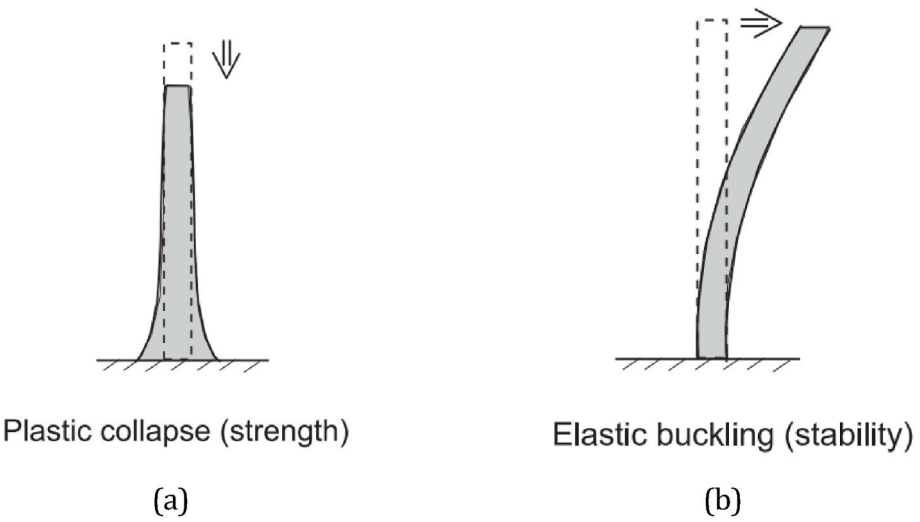

Fig. 12. Wall failure mode during printing process (Suiker, 2018) (a) plastic collapse, which is dominant by material strength (b) elastic buckling, which is dominant by material stiffness.

$$\frac{\bar{l}_{cr}}{\bar{l}_p} < \overline{\Lambda} : \text{elastic buckling}$$

$$\frac{\bar{l}_{cr}}{\bar{l}_p} > \overline{\Lambda} : \text{plastic collpase} \qquad \text{Eq. 10}$$

$$with\ \overline{\Lambda} = \left(\frac{h}{D_0}\right)\frac{\sigma_{p,0}}{(pg)^{2/3}}$$

In which, the dimensionless parameter Λ refers to "failure mechanism indicator". Based on this model, the failure mechanism is codetermined by a series of factors, including wall thickness h, initial material yield strength $\sigma_{p,0}$, initial bending stiffness D_0 of the printed wall structure, material density ρ and the gravitational acceleration g.

In contrast to other analytical models, this mechanical model studies the impact of more influencing factors on buildability. Several printing geometries, including the wall structure (Suiker, 2018), rectangular (Wolfs and Suiker, 2019), and square structures (Suiker et al., 2020) have been used for model validation. This model predicts the experimentally derived critical printing height quantitatively.

The primary advantages of Suiker's model lie in its simplicity of use and time efficiency. However, this model has the same limitation as other analytical models, e.g., being applicable only for specific printing geometries. Additionally, it does not apply to printing geometries other than wall structures. In contrast, numerical models can explore the impact of geometric features and material heterogeneity on structural analysis during the printing process. Such kind of tools also can replace or at least reduce the resource and time consuming trial-and-error testing. Thus, it is essential to present the numerical tools for buildability quantification. After material deposition, the printed filaments are at rest, behaving roughly like elasto-visco-plastic materials subject to gravitational loading. Two kinds of theories, namely, fluid and solid mechanics, have been adopted in numerical models.

3.3. Numerical models

Computational fluid dynamics (CFD) models based on fluid mechanics have been used to investigate the effect of constitutive relationships (such as generalized Newtonian fluid and elasto-visco-plastic fluid) on cross-sectional geometry of a printed layer (Mollah et al., 2021), as shown in Fig. 13. Furthermore, the relationship between the layer geometry and a series of printing parameters, including printing velocity and nozzle height, has been studied as well (Serdeczny et al., 2019; Comminal et al., 2019, 2020; Wolfs et al., 2021). The CFD is

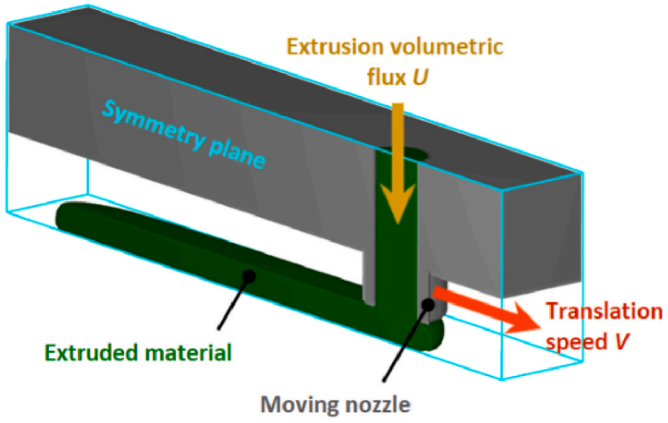

Fig. 13. A schematic diagram of 3D printing simulation using the CFD model (Comminal et al., 2019).

capable of describing the filament instability and tearing induced by the imbalance between the nozzle movement velocity and the material flow (as shown in Fig. 14), enabling the design of an optimal extrusion process (Wolfs et al., 2021). In addition, a CFD model has also been used to simulate the non-uniform material deposition at corners during printing process, as illustrated in Fig. 15. So far, the majority of CFD models focused on the extrusion process or geometry prediction of a single printing layer. Recently, the stability and deformation of multiple layers are simulated as well by means of this method, as shown in Fig. 16. However, CFD models have not been used for buildability quantification.

To better understand the structural failure during printing process, a Finite element method (FEM) based model using the ABAQUS package has been developed by Wolfs et al. (Wolfs et al., 2018, 2019; Wolfs and Suiker, 2019) to quantify the structural buildability. This 3D printing model can simulate two typical failure modes, i.e, plastic collapse and elastic buckling, during printing process. The time-dependent material characteristics and Mohr-Coulomb failure criterion are employed for plastic collapse simulation. The material properties are derived from uniaxial compression and shear tests performed at different material ages. This 3D printing model applies the model change option in ABAQUS to mimic layer-by-layer extrusion printing process. In each analysis step, material properties (strength and stiffness in this case) develop with the printing time to account for the impact of hydration. A

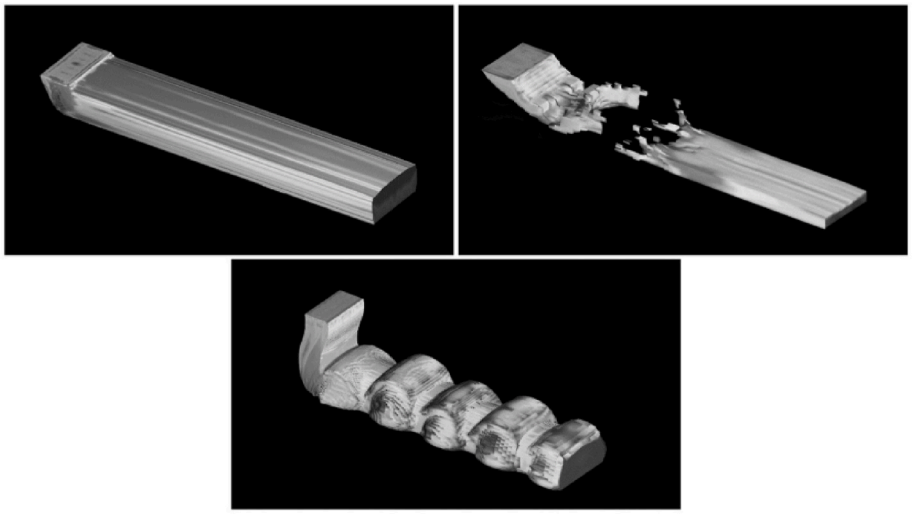

Fig. 14. Simulation of individual layer printing using CFD with possible printing results, i.e., nominal extrusion, filament tearing and filament buckling (Wolfs et al., 2021).

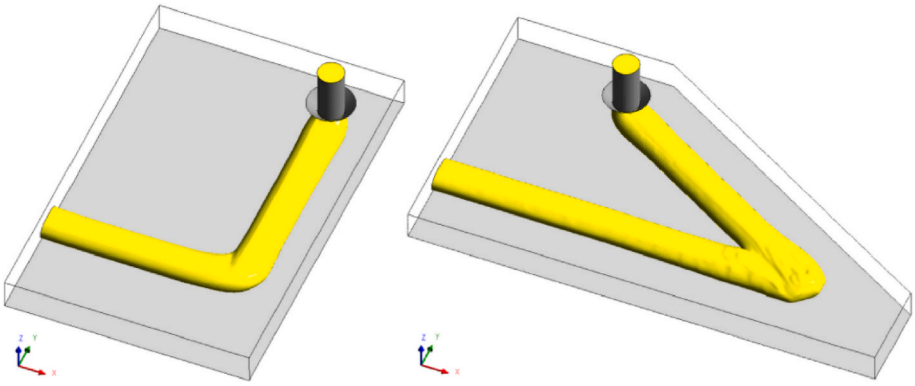

Fig. 15. Simulation of material deposition at corner during printing process; the left is the ideal material deposition with the corner equal to 90-degree and the right one is the non-ideal material deposition with the corner equal to 30-degree.

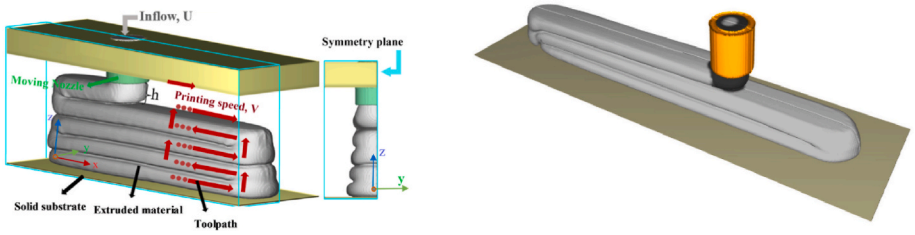

Fig. 16. Simulation of stability and deformation of muti-layers in 3D concrete printing using CFD model (a) a wall with five layers (Mollah et al., 2021); (b) a numerical case with three layers (Comminal et al., 2020).

geometric nonlinear analysis is carried out to consider the impact of large deformation on the structural analysis. Once any point of the printed structure reaches the material strength, the printed structure is regarded as having failed and the critical printed height is calculated. This model can qualitatively reproduce the experimental results, as shown in Fig. 17. However, there is a large quantitative disagreement with the printing experiment, almost 60%. This difference is mainly due to the discarding of localized damage, stress redistribution, and non-uniform gravitational loading. In terms of bucking, Wolfs et al. (2019) first performed linear buckling analysis to get possible buckling modes. An initial imperfection based on the first-mode instability was obtained and then incorporated into the numerical model for nonlinear buckling analysis. A good quantitative agreement with printing test was obtained. However, the buckling failure modes produced by the FEM-based method are different from those observed from the printing tests, as shown in Fig. 18. For a wall structure, an asymmetric buckling failure mode can be observed from experiment, which is different from the symmetric failure mode in the numerical analysis. For a rectangular layout, the buckling failure occurs close to the end of the structure while the numerical model predicts buckling failure in the middle of the

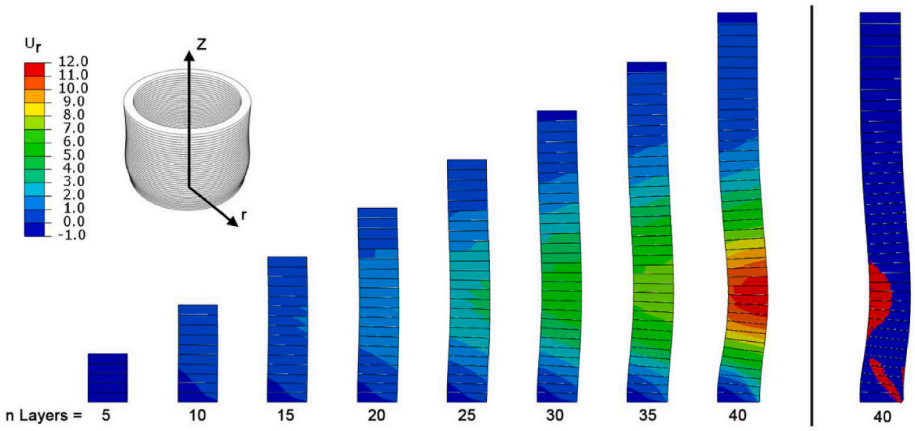

Fig. 17. FEM-based numerical model for plastic collapse failure model simulation vis hollow cylinder structure (Wolfs et al., 2018).

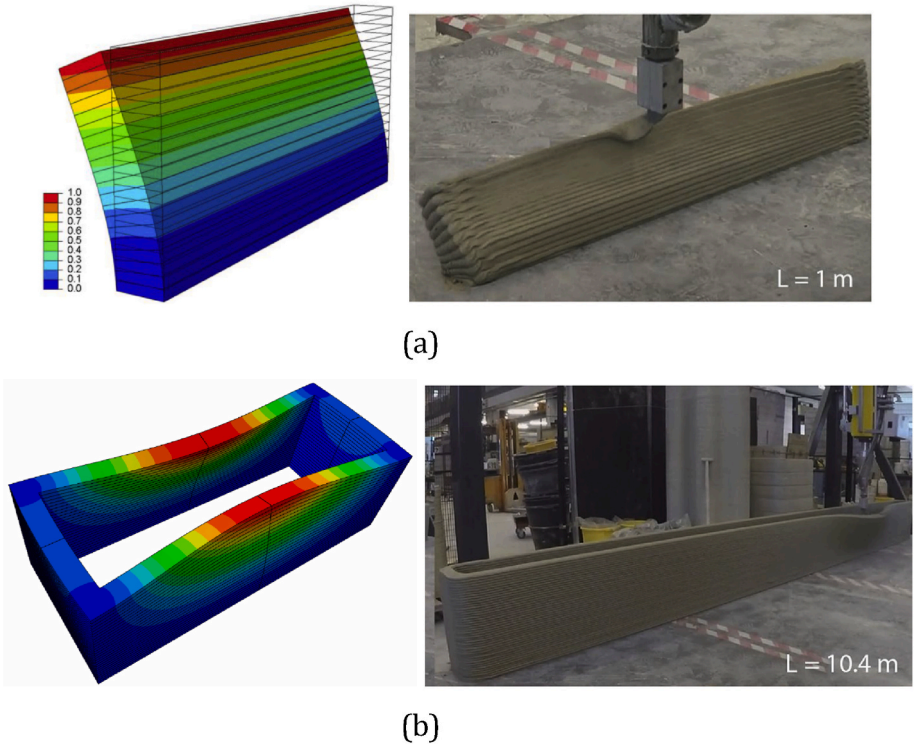

Fig. 18. Typical buckling failure mode during printing process (Wolfs, 2019) (a) wall structure (b) rectangular structure [In each subfigure, the left is the numerical analysis and the right is the experimental result].

rectangular structure. A possible reason to these differences is the fact that non-uniform gravitational loading in 3D printing simulations has been ignored. The buckling failure mode of analyzed object is determined by the initial imperfection in the numerical analyses. To reproduce the experimentally observed failure mode for elastic buckling, researchers from Ghent university (Ghent, 2019) tried to incorporate the non-uniform gravitational loading into the buckling analysis of wall structures, and derived an asymmetric buckling failure However, no published work describes the relationship between the non-uniform gravitational loading, geometric nonlinearity and buckling failure during printing process. Previous studies demonstrate that the FEM-based models can reproduce the experimentally derived results for 3D concrete printing. However, some model limitations still exist and need to be addressed.

Building upon FE models described above, Ooms et al. (Ooms et al., 2021; Vantyghem et al., 2020, 2021) proposed a parametric tool to create input files for 3D printing models without extensive manual modelling. This parametric tool automizes pre-processing step for structural analysis of 3DCP, especially for complex printing geometries. The general methodology of this parametric tool is shown in Fig. 19. Using this technique, they split each printing layer into several segments and studied the influence of non-uniform gravitational loading on failure height. Furthermore, they also investigated how different interaction methods (i.e., the tie constraints and contact-based interactions) affect structural deformation. A schematic diagram of these two interaction methods can be found in Fig. 20. In addition, they investigated the model change interaction for structural analysis during printing process, which allows for the simulation of deactivation and reactivation of printed segments. Their work shows: if 3D printing model based on ABAQUS is used, the option (i.e., model change interaction with strain) is the only choice with regards to printing process.

Similar to Ooms et al.'s research, Nguyen-Van et al. presented a

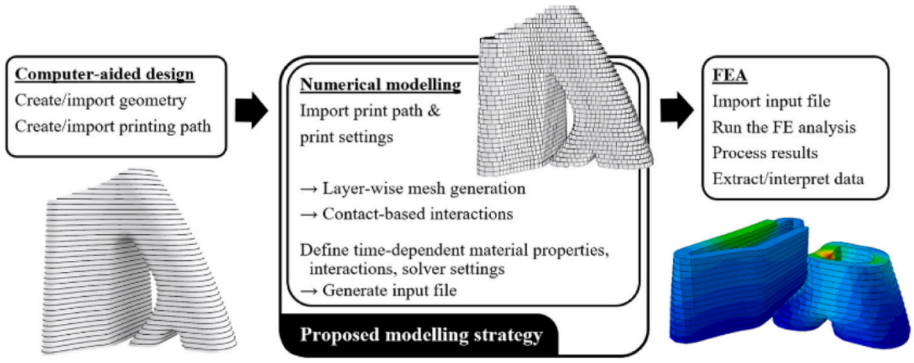

Fig. 19. General methodology of the proposed method for 3DCP simulation (Ooms et al., 2021).

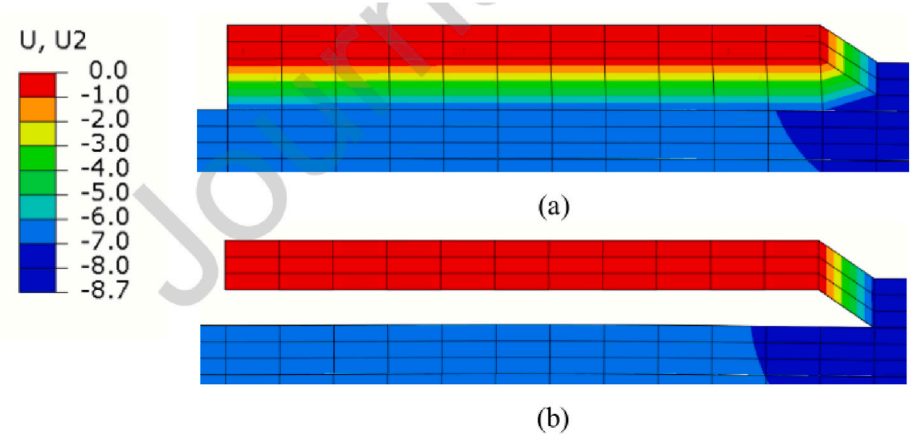

Fig. 20. Different interactions in ABAQUS: (a) tie constraints (b) contact-based interactions (Ooms et al., 2021).

novel computational framework to model structural buildability of complex triply periodic minimal surface via the given toolpath (Nguyen-Van et al., 2021). The general procedure is shown in Fig. 21. Using this technique, the influence of printing speed on the critical printed height and vertical deformation is studied.

Other studies have been performed to analyze influencing factors

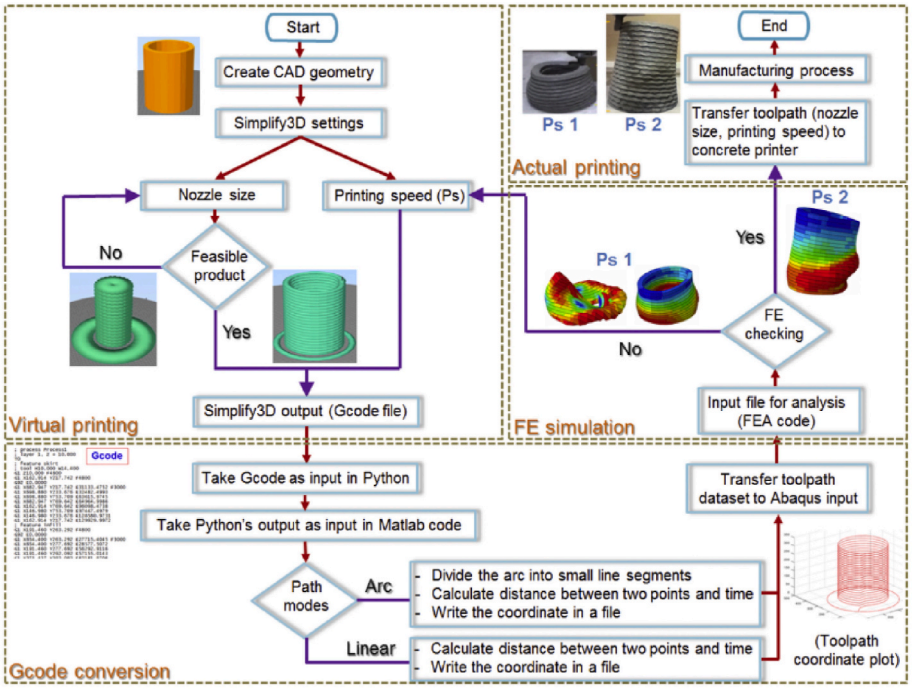

Fig. 21. The general procedure for the computational framework for 3D concrete printing (Nguyen-Van et al., 2021).

during the printing process. This includes improved FEM models (Ooms et al., 2021; Vantyghem et al., 2020; Wang et al.) and other novel methods (Chang et al., 2021; Ooms et al., 2021; Vantyghem et al., 2021; Nedjar, 2021). For instance, Nedjar (2022) incorporated the viscosity and geometric nonlinearity into the FEM-based 3D printing model for buildability quantification to investigate the impact of viscoelasticity at finite strain on buildability quantification. In his model, viscosity refers to early age creep, which is simulated via an internal variable method. The evolution of early creep is modelled through a generalized Maxwell model. Furthermore, the incremental algorithm is also incorporated into his model based on the Lagrangian formulation for buildability quantification. For model validation, a hollow cylinder structure and a wall structure were used. In terms of these two printing geometries, the predicted structural failure modes can be found in Fig. 22. The biggest improvement of this model is the incorporation of the viscosity of printable cementitious materials into the 3D printing model. The localized damage and non-uniform gravitational loading during printing process are not taken into account. Besides, the viscosity adopted in these numerical analyses does not correspond to that of a printable cementitious materials.

Besides Nedjar's 3D printing model with incremental viscoelasticity, a chemo-mechanical FEM model was presented for buildability quantification of 3DCP (Wang et al.). This model accounts for several important features of printable concrete at a fresh stage, including early-age creep, plasticity, and ageing due to hydration. In particular, the hydration process of cementitious material after deposition is described by a modified affinity hydration model. The contribution of this model studies the impact of chemical reaction on structural analysis during printing process.

In addition to FEM-based 3D printing model, Particle Finite Element Method (Reinold et al., 2022) has also been used for layer shape prediction and optimization of printing parameters. This method is Lagrangian-based Particle Finite Element Method using a Bingham constitutive model. This approach allowed for the numerical analysis of flow processing simulations with different process and material parameters. Laboratory 3D-printing experiments which measure the layer geometries are used for model validation. The numerical result can be found in Fig. 23. However, similar to the CFD approach, the model is only used to simulate the deformed geometry of extruded layer. There is no published work about the buildability quantification through the CFD model.

Clearly, 3D printing models (summarized in Table 1) are beneficial tools for prediction of structural deformation and buildability quantification of 3DCP. However, based on the published research, most models simulate extrusion-based 3D printing process. As soon as any point of the printed structure reach the material strength, the structure is considered to have failed. In that way, these models might underestimate the critical printing height of printed structure because the material yielding might only locally occur and the stress-redistribution can happen to ensure the printed structure avoids failure. Additionally, 3DCP is a continuous printing process, in which the gravitational load is gradually applied to the printed system. Thus, non-uniform stress distribution may occur. In addition, the printing material undergoes a layer-by-layer extrusion. A 3D printing process will likely cause the material to have more variable mechanical properties (such as strength and stiffness) compared to casting process. (Wolfs et al., 2019). Due to the material variation and non-uniform gravitational loading, some localized damage may occur, thereby affecting structural buildability. However, till now, no method considering these factors is found in the published literature. It is necessary to incorporate the material heterogeneity, non-uniform gravitational loading, localized damage and stress redistribution into 3D printing model for buildability quantification.

In FEM-based model, in order to simulate elastic buckling during printing process, a bifurcation linear buckling analysis is first conducted to get the geometric imperfection. Then, this imperfection is introduced into initial model for non-linear buckling analysis (Wolfs et al., 2019). In that case, only symmetric buckling failure modes can be obtained. To reproduce the experimentally observed asymmetric buckling failure, a new method with the incorporation of geometric nonlinearity should be developed.

The numerical models based on solid mechanics rely on the assumption that the behaviour of the material is elasto-plastic. This implies that only instantaneous strain is considered during the printing process, while time-dependent deformation is neglected. This delayed

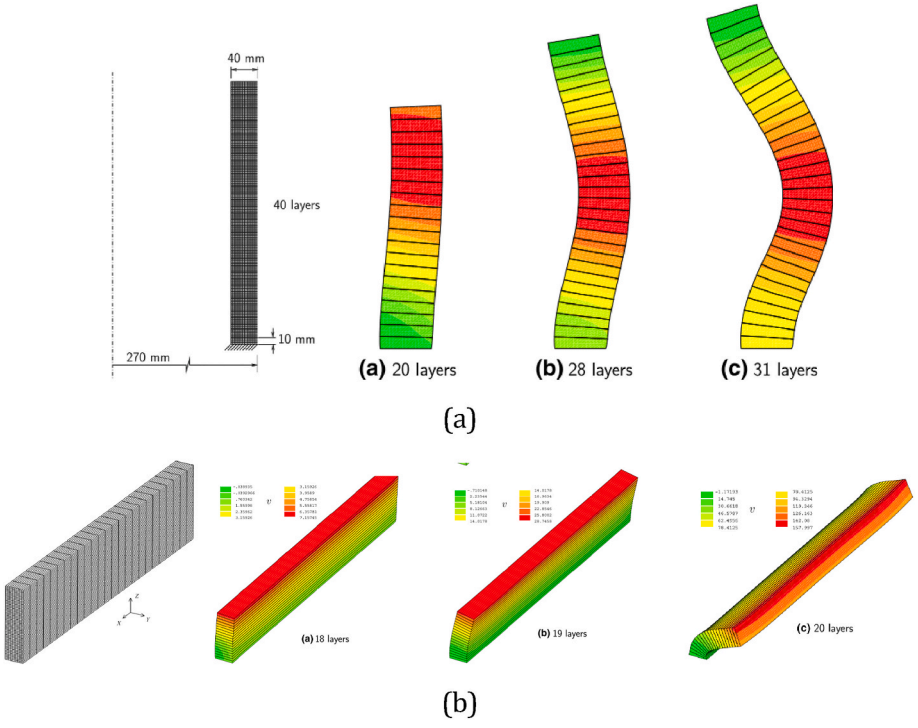

Fig. 22. FEM-based model for buildability quantification (a) hollow cylinder (b) wall structure (Nedjar, 2022).

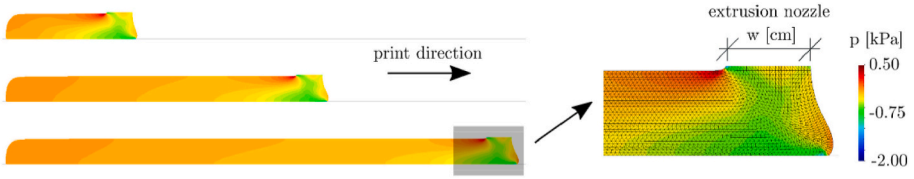

Fig. 23. Stress distribution of numerical analysis of a single printing layer after material deposition using Particle Finite Element Method (Reinold et al., 2022).

Table 1
Summary of all kinds of methods for buildability quantification in 3DCP (Chang et al., 2021, 2022b).

	Theory	Model introduction	Application	Limitation	Main contributors	Others
1	Rheology Analytical model	Rheological model considering flocculation-induced thixotropy and chemical reaction	Analytical models consider the development of materials properties and printing speed to predict structural failure due to plastic collapse	Geometry limitation, structural variability	Roussel (Roussel, 2018)	(Moini et al., 2022; Di Carlo et al., 2013; Cardoso et al., 2009; Chen et al., 2018; Jeong et al., 2019; Jayathilakage et al., 2019)
		Rheological model considers re-flocculation and structuration mechanisms			Kruger et al. (Kruger et al., 2019a, 2019d, 2019f)	
		An empirical model considering two curing functions for material development, i.e., linear and non-linear			Perrort et al. (Perrot et al., 2016)	
2	Solid mechanics Analytical model	A mechanistic model predicts elastic buckling and plastic collapse of wall structure based on different boundary conditions	The model analyses influence of printing velocity, curing function, geometrical features, and material heterogeneity		Suiker (Suiker et al., 2020; Suiker, 2018)	(Di Carlo et al., 2013; Panda et al., 2019c)
3	CFD Numerical model	CFD-based models with generalized Newtonian fluid and elastic-viscous-plastic fluid constitutive relationship	The CFD-based model predicts the cross-sectional shape of printing segments with the input parameters, including printing velocity, nozzle height, and extrusion force is established	Buckling failure, localized damage	R. Comminal et al. (Mollah et al., 2021; Serdeczny et al., 2019; Comminal et al., 2020)	Wolfs et al. (2021)
4	Solid mechanics Numerical model	FEM-based numerical model	Plastic collapse and elastic buckling	Localized damage, stress redistribution, Cold joint, moisture transfer	Wolfs et al. (Wolfs et al., 2018, 2019; Wolfs and Suiker, 2019)	(Jayathilakage et al., 2019; Ooms et al., 2021; Vantyghem et al., 2021; Wang et al.; Jayathilakage et al., 2021; Jayathilakage et al., 2020; Mengesha et al., 2020)
		Incremental viscoelasticity at finite strains for the modelling of 3D concrete			Nedjar (Nedjar, 2022)	(Wang et al.)
		Chemical-mechanical model	Plastic collapse and elastic buckling with the consideration of viscosity and hydration		Wang et al. (Wang et al.)	
		3D printing model based on lattice model	Plastic collapse and elastic buckling with the consideration of localized damage and early-age creep	Cold joint, moisture transfer	Chang et al. (Chang et al., 2021, 2022b, 2022c, 2023a, 2023b)	

deformation is induced by the creep, plastic and autogenous shrinkage, and consolidation settlement under distributed compressive loading and increases with printing time. Herein, the terminology 'early-age creep' is used to describe time-dependent deformation during printing process. In the published research, several early-age creep tests of 3D printable mortar/paste have been performed (Chen et al., 2019; Esposito et al., 2021); experiments indicate that early-age creep makes for about 7% of the viscoelastic deformation of the tested sample (Esposito et al., 2021). Therefore, early-age creep needs to be introduced into 3D printing model to explore its influence on the prediction of structural deformation and the buildability quantification.

Some of these issues have been tackled recently. To study the impact of localized damage occurred during build-up stage, a 3D printing model based on the lattice approach is proposed. This numerical model includes several factors, including the printing velocity, time-dependent material stiffness and strength, non-uniform gravitational loading and localized damage. It can reproduce two typical failure modes, i.e., plastic collapse and elastic buckling failure modes, which are similar to experimental findings (as shown in Fig. 24). In addition, the critical printing heights obtained from these numerical analyses are close to experimental results. Recently, early-age creep behaviour of 3D printable mortar measured via cyclic compressive loading test (Chang et al., 2022a) has been incorporated into this model to study the impact of early-age creep on buildability quantification.

The numerical methods show promising future on buildability quantification of 3DCP. However, those published models have their limitations and further research is required for model improvement.

First, these 3D printing models do not study the influence of cold joints or the high porosity in the interface zone, which may occur due to water loss and hydration process. Thus, these models are only suitable to printing cases with short printing time in which the cold joint effect can be ignored. To predict the structural behaviour of printing cases with long printing time, in the future, the impact of cold joints should be included.

In addition, as discussed before, one of the advantages of 3DCP is to eliminate the use of formwork. This leads to high water loss during the manufacturing process. As a result, more localized damage may occur due to plastic shrinkage (Roussel, 2006, 2018; Mohan et al., 2021; Khan

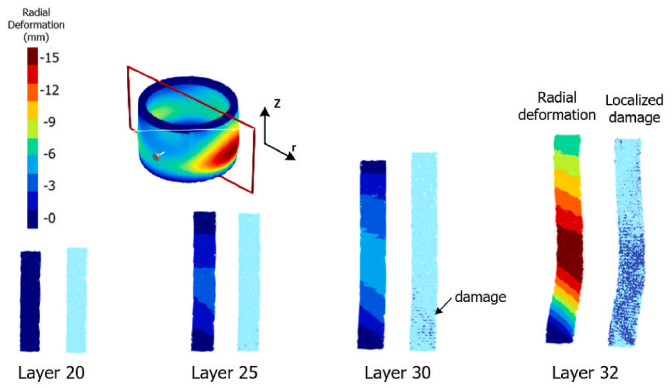

(a)

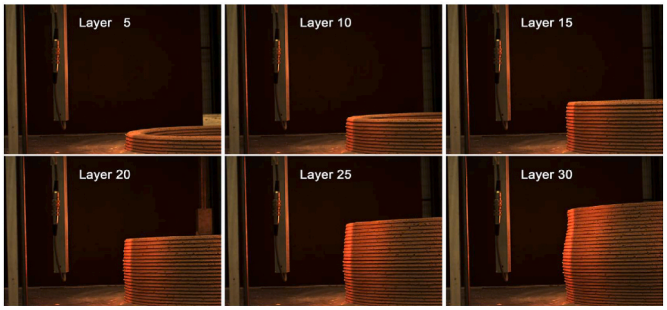

(b)

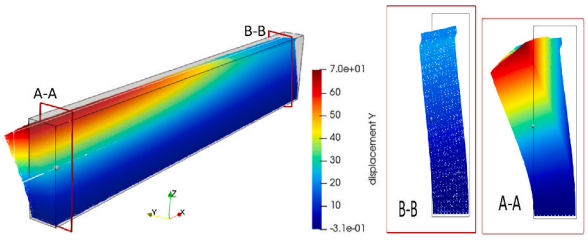

(c)

(d)

Fig. 24. Typical failure modes during printing process (a) lattice modelling of hollow cylinder structure (Chang et al., 2022b) (b) Experimental result of hollow cylinder structure (Wolfs et al., 2018) (c) lattice modelling of wall structure (Chang et al., 2022c) (d) Experimental result of wall structure (Wolfs et al., 2019).

et al., 2020; Nerella et al., 2019b). Therefore, incorporating the impact of moisture transfer into 3D printing model is also recommended.

Given that there is a stand-off distance during extrusion process, an additional compressive force sometimes occurs. For example, if the standoff distance is smaller than the layer height, local compression may occur, thereby affecting the structural stability and mechanical properties through interlayer porosity. To the best of the authors' knowledge, no published literature focused on such loading. Further research is recommended to investigate its influence on the structural behavior during the printing process.

Besides, all proposed numerical methods have limited applications. The CFD-based models mainly focus on the extrusion process while the solid mechanics-based models apply for the build-up stage. No numerical tool can simulate the whole printing process, from mixing and pumping to build-up stage. Developing such a model would give a deep insight into the impact of material properties (viscosity, stiffness and strength) on printability (pumpability and buildability).

4. Conclusions

This work summarizes the basic principles of different stages in 3DCP, which include pumping, extrusion, and building-up process. A review of the current strategies for buildability quantification is given from three aspects. Experiments and analytical methods for buildability quantification of 3DCP have been proposed in the literature. However, experiments are labour-and-time consuming, while the applicability of analytical models is limited to specific printing geometries. Based on the presented state of art on methods for buildability quantification of 3DCP, some conclusions can be drawn:

- The rheological models can investigate the material failure during the printing process from the perspective of chemical reaction and physical origin. This kind of model can capture the intricate nature of the underlying failure mechanisms. However, it is difficult to allow for the geometry impact on structural failure. In contract, the model based on solid mechnics is able to investigate the impact of geometry on structural failure.
- A reliable numerical model can be utilized to investigate the structural behaviour and optimize the printing parameters and material design. However, there are obvious limitations to current numerical models. Some important factors such as cold joint formation and moisture transfer have not been considered. More efforts are needed in the development and improvement of numerical methods for the buildability quantification of 3DCP.
- In terms of 3D printing, there are two typical printing method, i.e, the laminar flow and non-laminar flow. One difference between these two printing methods focuses on the existence of compressive force from the nozzle. However, this kind of force have not been considered for the buildaibility quantification. Further research is recommended to fill this research gap.
- Due to the relative simplicity of current 3D printing models, almost all the reviewed models only take the time-dependent stiffness and strength into account for buildability quantification. The time-dependent behaviours such as early-age creep and shrinkage may also significantly affect structural buildability and should be analyzed.
- All proposed numerical methods have limited applications. There is no numerical method that can predict the performance of printed cementitious materials during the whole printing process. Developing such kind of model could give a deep insight into the influence of material properties (viscosity, stiffness and strength) on printability (pumpability and buildability).

Declaration of competing interest

The authors declare that they have no known competing financial interests or personal relationships that could have appeared to influence the work reported in this paper.

Data availability

Data will be made available on request.

Acknowledgements

Ze Chang would like to acknowledge the funding supported by China Scholarship Council under grant number 201806060129. Branko Šavija acknowledge the financial support of the European Research Council (ERC) within the framework of the ERC Starting Grant Project "Auxetic Cementitious Composites by 3D printing (ACC-3D)", Grant Agreement Number 101041342.

References

Asprone, D., Auricchio, F., Menna, C., Mercuri, V., 2018. 3D printing of reinforced concrete elements: technology and design approach. Construct. Build. Mater. 165, 218–231.
Batikha, M., Jotangia, R., Baaj, M.Y., Mousleh, I., 2022. 3D concrete printing for sustainable and economical construction: a comparative study. Autom. ConStruct. 134, 104087.
Bonoli, A., Zanni, S., Serrano-Bernardo, F., 2021. Sustainability in building and construction within the framework of circular cities and european new green deal. The contribution of concrete recycling. Sustainability 13 (4), 2139.
Bos, F., Wolfs, R., Ahmed, Z., Salet, T., 2016. Additive manufacturing of concrete in construction: potentials and challenges of 3D concrete printing. Virtual Phys. Prototyp. 11 (3), 209–225.
Bos, F.P., Lucas, S.S., Wolfs, R.J., Salet, T.A., 2020. Second RILEM International Conference on Concrete and Digital Fabrication: Digital Concrete 2020. Springer Nature.
Briffaut, M., Benboudjema, F., Torrenti, J.-M., Nahas, G., 2012. Concrete early age basic creep: experiments and test of rheological modelling approaches. Construct. Build. Mater. 36, 373–380.
Buswell, R.A., de Silva, W.L., Jones, S., Dirrenberger, J., 2018. 3D printing using concrete extrusion: a roadmap for research. Cement Concr. Res. 112, 37–49.
Buswell, Richard, Blanco, Ana, Cavalaro, Sergio, Kinnell, P., 2022. Third RILEM International Conference on Concrete and Digital Fabrication. Springer.
Cao, X., Yu, S., Cui, H., Li, Z., 2022. 3D printing devices and reinforcing techniques for extruded cement-based materials: a review. Buildings 12 (4), 453.
Cardoso, F.A., John, V.M., Pileggi, R.G., 2009. Rheological behavior of mortars under different squeezing rates. Cement Concr. Res. 39 (9), 748–753.
Casagrande, L., Esposito, L., Menna, C., Asprone, D., Auricchio, F., 2020. Effect of testing procedures on buildability properties of 3D-printable concrete. Construct. Build. Mater. 245, 118286.
Chang, Z., Xu, Y., Chen, Y., Gan, Y., Schlangen, E., Šavija, B., 2021. A discrete lattice model for assessment of buildability performance of 3D-printed concrete. Comput. Aided Civ. Infrastruct. Eng. 36 (5), 638–655.
Chang, Z., Liang, M., Xu, Y., Wan, Z., Schlangen, E., Šavija, B., 2022a. Early-age creep of 3D printable mortar: experiments and analytical modelling. Cement Concr. Compos. 138.
Chang, Z., Liang, M., Xu, Y., Schlangen, E., Šavija, B., 2022b. 3D concrete printing: lattice modeling of structural failure considering damage and deformed geometry. Cement Concr. Compos., 104719
Chang, Z., Zhang, H., Liang, M., Schlangen, E., Šavija, B., 2022c. Numerical simulation of elastic buckling in 3D concrete printing using the lattice model with geometric nonlinearity. Autom. ConStruct. 142, 104485.
Chang, Z., Liang, M., He, S., Schlangen, E., Šavija, B., 2023a. Lattice Modelling of Early-Age Creep of 3D Printed Segments with the Consideration of Stress History. Materials & Design, 112340.
Chang, Z., Liang, M., Chen, Y., Schlangen, E., Šavija, B., 2023b. Does Early Age Creep Influence Buildability of 3D Printed Concrete? Insights from Numerical Simulations. Additive Manufacturing, 103788.
Chen, M., Li, L., Zheng, Y., Zhao, P., Lu, L., Cheng, X., 2018. Rheological and mechanical properties of admixtures modified 3D printing sulphoaluminate cementitious materials. Construct. Build. Mater. 189, 601–611.
Chen, Y., Li, Z., Chaves Figueiredo, S., Çopuroğlu, O., Veer, F., Schlangen, E., 2019. Limestone and calcined clay-based sustainable cementitious materials for 3D concrete printing: a fundamental study of extrudability and early-age strength development. Appl. Sci. 9 (9), 1809.
Chen, M., Yang, L., Zheng, Y., Huang, Y., Li, L., Zhao, P., Wang, S., Lu, L., Cheng, X., 2020. Yield stress and thixotropy control of 3D-printed calcium sulfoaluminate cement composites with metakaolin related to structural build-up. Construct. Build. Mater. 252, 119090.
Choi, M., Roussel, N., Kim, Y., Kim, J., 2013. Lubrication layer properties during concrete pumping. Cement Concr. Res. 45, 69–78.
Choi, M., Park, K., Oh, T., 2016. Viscoelastic properties of fresh cement paste to study the flow behavior. International Journal of Concrete Structures and Materials 10 (3), 65–74.
Comminal, R., Serdeczny, M.P., Ranjbar, N., Mehrali, M., Pedersen, D.B., Stang, H., Spangenberg, J., 2019. Modelling of material deposition in big area additive manufacturing and 3D concrete printing. Joint Special Interest Group Meetin g between Euspen and ASPE Advancing Precision in Additive Manufacturing, Th e European Society for Precision Engineering and Nanotechnology 151–154.
Comminal, R., da Silva, W.R.L., Andersen, T.J., Stang, H., Spangenberg, J., 2020. Modelling of 3D concrete printing based on computational fluid dynamics. Cement Concr. Res. 138, 106256.
Cui, H., Li, Y., Cao, X., Huang, M., Tang, W., Li, Z., 2022. Experimental study of 3D concrete printing configurations based on the buildability evaluation. Appl. Sci. 12 (6), 2939.
Das, A., Song, Y., Mantellato, S., Wangler, T., Flatt, R.J., Lange, D.A., 2020. Influence of Pumping/extrusion on the Air-Void System of 3D Printed Concrete, RILEM International Conference on Concrete and Digital Fabrication. Springer, pp. 417–427.
De Schutter, G., Feys, D., 2016. Pumping of fresh concrete: insights and challenges. RILEM Technical Letters 1, 76–80.
de Soto, B.G., Agustí-Juan, I., Hunhevicz, J., Joss, S., Graser, K., Habert, G., Adey, B.T., 2018. Productivity of digital fabrication in construction: cost and time analysis of a robotically built wall. Autom. ConStruct. 92, 297–311.
De Vlieger, J., Boehme, L., Blaakmeer, J., Li, J., 2023. Buildability assessment of mortar with fine recycled aggregates for 3D printing. Construct. Build. Mater. 367, 130313.
Dey, D., Srinivas, D., Panda, B., Suraneni, P., Sitharam, T., 2022. Use of industrial waste materials for 3D printing of sustainable concrete: a review. J. Clean. Prod., 130749
Di Carlo, T., Khoshnevis, B., Carlson, A., 2013. Experimental and Numerical Techniques to Characterize Structural Properties of Fresh Concrete, ASME International Mechanical Engineering Congress and Exposition. American Society of Mechanical Engineers. V009T10A062.
Economic, U.N.D.o., Division, S.A.P., 1999. World Population Prospects: the 1998 Revision. United Nations Publications.
El Cheikh, K., Rémond, S., Khalil, N., Aouad, G., 2017. Numerical and experimental studies of aggregate blocking in mortar extrusion. Construct. Build. Mater. 145, 452–463.
Esposito, L., Casagrande, L., Menna, C., Asprone, D., Auricchio, F., 2021. Early-age creep behaviour of 3D printable mortars: experimental characterisation and analytical modelling. Mater. Struct. 54 (6), 1–16.
Feys, D., 2019. How much is bulk concrete sheared during pumping? Construct. Build. Mater. 223, 341–351.
Feys, D., Khayat, K.H., Khatib, R., 2016a. How do concrete rheology, tribology, flow rate and pipe radius influence pumping pressure? Cement Concr. Compos. 66, 38–46.
Feys, D., De Schutter, G., Khayat, K.H., Verhoeven, R., 2016b. Changes in rheology of self-consolidating concrete induced by pumping. Mater. Struct. 49 (11), 4657–4677.
Gerbert, P., Castagnino, S., Rothballer, C., Renz, A., F, R., 2016. The Transformative Power of Building Information Modeling. March 08).
Ghent, C.D., 2019. Numerical Simulation of 3D Concrete Printing Processes.
Ghent, C.D., 2020. Elastic Buckling vs Plastic Collapse in Concrete Printing. Youtube. https://www.youtube.com/watch?v=2FdlRk_79x4&t=1s.
Harty, C., 2008. Implementing innovation in construction: contexts, relative boundedness and actor-network theory. Construct. Manag. Econ. 26 (10), 1029–1041.
Hass, L., Bos, F., 2020. Bending and pull-out tests on a novel screw type reinforcement for extrusion-based 3D printed concrete. In: RILEM International Conference on Concrete and Digital Fabrication. Springer, pp. 632–645.
He, Y., Zhang, Y., Zhang, C., Zhou, H., 2020. Energy-saving potential of 3D printed concrete building with integrated living wall. Energy Build. 222, 110110.
Jayathilakage, R., Sanjayan, J., Rajeev, P., 2019. Direct shear test for the assessment of rheological parameters of concrete for 3D printing applications. Mater. Struct. 52 (1), 1–13.
Jayathilakage, R., Rajeev, P., Sanjayan, J., 2020. Yield stress criteria to assess the buildability of 3D concrete printing. Construct. Build. Mater. 240, 117989.
Jayathilakage, R., Rajeev, P., Sanjayan, J., 2021. Extrusion rheometer for 3D concrete printing. Cement Concr. Compos. 121, 104075.
Jeong, H., Han, S.-J., Choi, S.-H., Lee, Y.J., Yi, S.T., Kim, K.S., 2019. Rheological property criteria for buildable 3D printing concrete. Materials 12 (4), 657.
Jo, S.D., Park, C.K., Jeong, J.H., Lee, S.H., Kwon, S.H., 2012. A computational approach to estimating a lubricating layer in concrete pumping. Comput. Mater. Continua (CMC) 27 (3), 189.
Jo, J.H., Jo, B.W., Cho, W., Kim, J.-H., 2020. Development of a 3D printer for concrete structures: laboratory testing of cementitious materials. International Journal of Concrete Structures and Materials 14 (1), 1–11.
Joh, C., Lee, J., Bui, T.Q., Park, J., Yang, I.-H., 2020. Buildability and mechanical properties of 3D printed concrete. Materials 13 (21), 4919.
Kaplan, D., de Larrard, F., Sedran, T., 2005. Design of concrete pumping circuit. ACI Mater. J. 102 (2), 110.
Kazemian, A., Yuan, X., Cochran, E., Khoshnevis, B., 2017. Cementitious materials for construction-scale 3D printing: laboratory testing of fresh printing mixture. Construct. Build. Mater. 145, 639–647.
Kazemian, A., Yuan, X., Davtalab, O., Khoshnevis, B., 2019. Computer vision for real-time extrusion quality monitoring and control in robotic construction. Autom. ConStruct. 101, 92–98.
Khan, M.S., Sanchez, F., Zhou, H., 2020. 3-D printing of concrete: beyond horizons. Cement Concr. Res. 133, 106070.
Kruger, J., Zeranka, S., van Zijl, G.J.C., Materials, B., 2019a. An ab initio approach for thixotropy characterisation of (nanoparticle-infused). 3D printable concrete 224, 372–386.
Kruger, J., Zeranka, S., van Zijl, G.J.A.i.C., 2019b. 3D Concrete Printing: a Lower Bound Analytical Model for Buildability Performance Quantification, vol. 106, 102904.
Kruger, J., van den Heever, M., Cho, S., Zeranka, S., van Zijl, G., 2019c. High-performance 3D printable concrete enhanced with nanomaterials. In: Proceedings of the International Conference on Sustainable Materials, Systems and Structures: New Generation of Construction Materials. RILEM Publications SARL Rovinj, Croatia, pp. 533–540.

Kruger, J., Zeranka, S., van Zijl, G., 2019d. 3D concrete printing: a lower bound analytical model for buildability performance quantification. Autom. ConStruct. 106, 102904.
Kruger, J., Zeranka, S., van Zijl, G., 2019e. An ab initio approach for thixotropy characterisation of (nanoparticle-infused) 3D printable concrete. Construct. Build. Mater. 224, 372–386.
Kruger, J., Zeranka, S., van Zijl, G., 2019f. Quantifying Constructability Performance of 3D Concrete Printing via Rheology-Based Analytical Models, Rheology and Processing of Construction Materials. Springer, pp. 400–408.
Kruger, J., du Plessis, A., van Zijl, G., 2021. An investigation into the porosity of extrusion-based 3D printed concrete. Addit. Manuf. 37, 101740.
Le, T.T., Austin, S.A., Lim, S., Buswell, R.A., Gibb, A.G., Thorpe, T., 2012. Mix design and fresh properties for high-performance printing concrete. Mater. Struct. 45 (8), 1221–1232.
Leal da Silva, W.R., Fryda, H., Bousseau, J.-N., Andreani, P.-A., Andersen, T.J., 2019. Evaluation of Early-Age Concrete Structural Build-Up for 3D Concrete Printing by Oscillatory Rheometry, International Conference on Applied Human Factors and Ergonomics. Springer, pp. 35–47.
Lecompte, T., Perrot, A., 2017. Non-linear modeling of yield stress increase due to SCC structural build-up at rest. Cement Concr. Res. 92, 92–97.
Ma, G., Buswell, R., da Silva, W.R.L., Wang, L., Xu, J., Jones, S.Z., 2022. Technology readiness: a global snapshot of 3D concrete printing and the frontiers for development. Cement Concr. Res. 156, 106774.
Maltese, C., Pistolesi, C., Bravo, A., Cella, F., Cerulli, T., Salvioni, D., 2007. A case history: effect of moisture on the setting behaviour of a Portland cement reacting with an alkali-free accelerator. Cement Concr. Res. 37 (6), 856–865.
Mechtcherine, V., Bos, F.P., Perrot, A., da Silva, W.L., Nerella, V., Fataei, S., Wolfs, R.J., Sonebi, M., Roussel, N., 2020a. Extrusion-based additive manufacturing with cement-based materials–Production steps, processes, and their underlying physics: a review. Cement Concr. Res. 132, 106037.
Mechtcherine, V., Michel, A., Liebscher, M., Schmeier, T., 2020b. Extrusion-based additive manufacturing with carbon reinforced concrete: concept and feasibility study. Materials 13 (11), 2568.
Mengesha, M., Schmidt, A., Göbel, L., Lahmer, T., 2020. Numerical modeling of an extrusion-based 3D concrete printing process considering a spatially varying pseudo-density approach. In: RILEM International Conference on Concrete and Digital Fabrication. Springer, pp. 323–332.
Mohan, M.K., Rahul, A., De Schutter, G., Van Tittelboom, K., 2021. Extrusion-based concrete 3D printing from a material perspective: a state-of-the-art review. Cement Concr. Compos. 115, 103855.
Moini, R., Olek, J., Zavattieri, P.D., Youngblood, J.P., 2022. Early-age buildability-rheological properties relationship in additively manufactured cement paste hollow cylinders. Cement Concr. Compos. 131, 104538.
Mollah, M.T., Comminal, R., Serdeczny, M.P., Pedersen, D.B., Spangenberg, J., 2021. Stability and Deformations of Deposited Layers in Material Extrusion Additive Manufacturing. Additive Manufacturing, 102193.
Nedjar, B., 2021. On a geometrically nonlinear incremental formulation for the modeling of 3D concrete printing. Mech. Res. Commun. 116, 103748.
Nedjar, B., 2022. Incremental viscoelasticity at finite strains for the modelling of 3D concrete printing. Comput. Mech. 69 (1), 233–243.
Nerella, V.N., Mechtcherine, V., 2019. Studying the printability of fresh concrete for formwork-free concrete onsite 3D printing technology (CONPrint3D). 3D Concrete Printing Technology 333–347. Elsevier.
Nerella, V., Näther, M., Iqbal, A., Butler, M., Mechtcherine, V., 2019a. Inline quantification of extrudability of cementitious materials for digital construction. Cement Concr. Compos. 95, 260–270.
Nerella, V.N., Hempel, S., Mechtcherine, V., 2019b. Effects of layer-interface properties on mechanical performance of concrete elements produced by extrusion-based 3D-printing. Construct. Build. Mater. 205, 586–601.
Nerella, V.N., Krause, M., Mechtcherine, V., 2020. Direct printing test for buildability of 3D-printable concrete considering economic viability. Autom. ConStruct. 109, 102986.
Nguyen-Van, V., Panda, B., Zhang, G., Nguyen-Xuan, H., Tran, P., 2021. Digital design computing and modelling for 3-D concrete printing. Autom. ConStruct. 123, 103529.
Ooms, T., Vantyghem, G., Van Coile, R., De Corte, W., 2021. A parametric modelling strategy for the numerical simulation of 3D concrete printing with complex geometries. Addit. Manuf. 38, 101743.
Panda, B., Tan, M.J., 2018. Experimental study on mix proportion and fresh properties of fly ash based geopolymer for 3D concrete printing. Ceram. Int. 44 (9), 10258–10265.
Panda, B., Paul, S.C., Mohamed, N.A.N., Tay, Y.W.D., Tan, M.J., 2018a. Measurement of tensile bond strength of 3D printed geopolymer mortar. Measurement 113, 108–116.
Panda, B., Unluer, C., Tan, M.J., 2018b. Investigation of the rheology and strength of geopolymer mixtures for extrusion-based 3D printing. Cement Concr. Compos. 94, 307–314.
Panda, B., Mohamed, N., Ahamed, N., Paul, S.C., Bhagath Singh, G., Tan, M.J., Šavija, B., 2019a. The effect of material fresh properties and process parameters on buildability and interlayer adhesion of 3D printed concrete. Materials 12 (13), 2149.
Panda, B., Singh, G.B., Unluer, C., Tan, M.J., 2019b. Synthesis and characterization of one-part geopolymers for extrusion based 3D concrete printing. J. Clean. Prod. 220, 610–619.
Panda, B., Lim, J.H., Tan, M.J., 2019c. Mechanical properties and deformation behaviour of early age concrete in the context of digital construction. Compos. B Eng. 165, 563–571.
Pang, B., Jin, Z., Zhang, Y., Liu, Z., She, W., Wang, P., Yu, Y., Zhang, X., Xiong, C., Li, N., 2022a. Ultraductile cementitious structural health monitoring coating: waterborne polymer biomimetic muscle and polyhedral oligomeric silsesquioxane-assisted C-S-H dispersion. Adv. Funct. Mater. 32 (51), 2208676.
Pang, B., Jin, Z., Zhang, Y., Xu, L., Li, M., Wang, C., Zhang, Y., Yang, Y., Zhao, P., Bi, J., 2022b. Ultraductile waterborne epoxy-concrete composite repair material: epoxy-fiber synergistic effect on flexural and tensile performance. Cement Concr. Compos. 129, 104463.
Paul, S.C., Tay, Y.W.D., Panda, B., Tan, M.J., 2018. Fresh and hardened properties of 3D printable cementitious materials for building and construction. Arch. Civ. Mech. Eng. 18 (1), 311–319.
Perrot, A., Pierre, A., Vitaloni, S., Picandet, V., 2015. Prediction of lateral form pressure exerted by concrete at low casting rates. Mater. Struct. 48 (7), 2315–2322.
Perrot, A., Rangeard, D., Pierre, A., 2016. Structural built-up of cement-based materials used for 3D-printing extrusion techniques. Mater. Struct. 49 (4), 1213–1220.
Perrot, A., Rangeard, D., Nerella, V.N., Mechtcherine, V., 2018. Extrusion of cement-based materials-an overview. RILEM Technical Letters 3, 91–97.
Perrot, A., Pierre, A., Nerella, V., Wolfs, R., Keita, E., Nair, S., Neithalath, N., Roussel, N., 2021. Mechtcherine, from analytical methods to numerical simulations: a process engineering toolbox for 3D concrete printing. Cement Concr. Compos. 122, 104164.
Pessoa, S., Guimarães, A.S., Lucas, S.S., Simões, N., 2021. 3D printing in the construction industry-A systematic review of the thermal performance in buildings. Renew. Sustain. Energy Rev. 141, 110794.
Qian, Y., Kawashima, S., 2016. Use of creep recovery protocol to measure static yield stress and structural rebuilding of fresh cement pastes. Cement Concr. Res. 90, 73–79.
Rauline, D., Le Blévec, J.-M., Bousquet, J., Tanguy, P., 2000. A comparative assessment of the performance of the Kenics and SMX static mixers. Chem. Eng. Res. Des. 78 (3), 389–396.
Reinold, J., Nerella, V.N., Mechtcherine, V., Meschke, G., 2022. Extrusion process simulation and layer shape prediction during 3D-concrete-printing using the Particle Finite Element Method. Autom. ConStruct. 136, 104173.
Reiter, L., Wangler, T., Roussel, N., Flatt, R.J., 2018. The role of early age structural build-up in digital fabrication with concrete. Cement Concr. Res. 112, 86–95.
Reiter, L., Wangler, T., Anton, A., Flatt, R.J., 2020. Setting on demand for digital concrete–principles, measurements, chemistry, validation. Cement Concr. Res. 132, 106047.
Roussel, N., 2006. A thixotropy model for fresh fluid concretes: theory, validation and applications. Cement Concr. Res. 36 (10), 1797–1806.
Roussel, N., 2018. Rheological requirements for printable concretes. Cement Concr. Res. 112, 76–85.
Roussel, N., Ovarlez, G., Garrault, S., Brumaud, C., 2012. The origins of thixotropy of fresh cement pastes. Cement Concr. Res. 42 (1), 148–157.
Roussel, N., Spangenberg, J., Wallevik, J., Wolfs, R., 2020. Numerical simulations of concrete processing: from standard formative casting to additive manufacturing. Cement Concr. Res. 135, 106075.
Salet, T., Ahmed, Z., Bos, F., Laagland, H., 2018. 3D Printed Concrete Bridge, 3rd International Conference on Progress in Additive Manufacturing. Pro-AM, pp. 2–9, 2018.
Sanjayan, J., Jayathilakage, R., Rajeev, P., 2021. Vibration induced active rheology control for 3D concrete printing. Cement Concr. Res. 140, 106293.
Serdeczny, M.P., Comminal, R., Pedersen, D.B., Spangenberg, J., 2019. Numerical simulations of the mesostructure formation in material extrusion additive manufacturing. Addit. Manuf. 28, 419–429.
Siddika, A., Mamun, M.A.A., Ferdous, W., Saha, A.K., Alyousef, R., 2020. 3D-printed concrete: applications, performance, and challenges. Journal of Sustainable Cement-Based Materials 9 (3), 127–164.
Suiker, A.S.J., 2018. Mechanical performance of wall structures in 3D printing processes: theory, design tools and experiments. Int. J. Mech. Sci. 137, 145–170.
Suiker, A.S., Wolfs, R.J., Lucas, S.M., Salet, T.A., 2020. Elastic buckling and plastic collapse during 3D concrete printing. Cement Concr. Res. 135, 106016.
Tao, Y., Rahul, A., Lesage, K., Yuan, Y., Van Tittelboom, K., De Schutter, G., 2021. Stiffening control of cement-based materials using accelerators in inline mixing processes: possibilities and challenges. Cement Concr. Compos. 119, 103972.
Tao, Y., Rahul, A., Mohan, M.K., Van Tittelboom, K., Yuan, Y., De Schutter, G., 2022a. Blending performance of helical static mixer used for twin-pipe 3D concrete printing. Cement Concr. Compos. 134, 104741.
Tao, Y., Mohan, M.K., Rahul, A., Yuan, Y., De Schutter, G., Van Tittelboom, K., 2022b. Stiffening controllable concrete modified with redispersible polymer powder for twin-pipe printing. Cement Concr. Res. 161, 106953.
Tay, Y.W.D., Qian, Y., Tan, M.J., 2019. Printability region for 3D concrete printing using slump and slump flow test. Compos. B Eng. 174, 106968.
Thakur, R., Vial, C., Nigam, K., Nauman, E., Djelveh, G., 2003. Static mixers in the process industries—a review. Chem. Eng. Res. Des. 81 (7), 787–826.
Ting, G.H.A., Quah, T.K.N., Lim, J.H., Tay, Y.W.D., Tan, M.J., 2022. Extrudable region parametrical study of 3D printable concrete using recycled glass concrete. J. Build. Eng. 50, 104091.
Vallurupalli, K., Farzadnia, N., Khayat, K.H.J.C., Composites, C., 2021. Effect of Flow Behavior and Process-Induced Variations on Shape Stability of 3D Printed Elements–A Review, 103952.
Vantyghem, G., Ooms, T., De Corte, W., 2020. FEM Modelling Techniques for Simulation of 3D Concrete Printing. arXiv preprint arXiv:.06907.
Vantyghem, G., Ooms, T., De Corte, W., 2021. VoxelPrint: a Grasshopper plug-in for voxel-based numerical simulation of concrete printing. Autom. ConStruct. 122, 103469.
Vosahlik, J., Riding, K.A., Feys, D., Lindquist, W., Keller, L., Van Zetten, S., Schulz, B., 2018. Concrete pumping and its effect on the air void system. Mater. Struct. 51 (4), 1–15.

Q. Wang, X. Ren, J. Li, A Chemo-Mechanical Model for Predicting the Buildability of 3d Printed Concrete, Available at: SSRN 4147420..
Wangler, T., Flatt, R.J., 2018. First RILEM International Conference on Concrete and Digital Fabrication–Digital Concrete, Springer2018.
Wangler, T., Lloret, E., Reiter, L., Hack, N., Gramazio, F., Kohler, M., Bernhard, M., Dillenburger, B., Buchli, J., Roussel, N., 2016. Digital concrete: opportunities and challenges. RILEM Technical Letters 1, 67–75.
Wangler, T., Roussel, N., Bos, F.P., Salet, T.A., Flatt, R.J., 2019. Digital concrete: a review. Cement Concr. Res. 123, 105780.
Wolfs, R., 2019. Experimental Characterization and Numerical Modelling of 3D Printed Concrete: Controlling Structural Behaviour in the Fresh and Hardened State. Eindhoven University of Technology.
Wolfs, R., Suiker, A., 2019. Structural failure during extrusion-based 3D printing processes. Int. J. Adv. Des. Manuf. Technol. 104 (1–4), 565–584.
Wolfs, R., Bos, F., Salet, T., 2018. Early age mechanical behaviour of 3D printed concrete: numerical modelling and experimental testing. Cement Concr. Res. 106, 103–116.
Wolfs, R., Bos, F., Salet, T.J.C., 2019. Triaxial compression testing on early age concrete for numerical analysis of 3D concrete printing. Cement Concr. Compos. 104, 103344.
Wolfs, R.J., Salet, T.A., Roussel, N., 2021. Filament geometry control in extrusion-based additive manufacturing of concrete: the good, the bad and the ugly. Cement Concr. Res. 150, 106615.
Zhang, J., Xu, S., Li, W., 2012. High shear mixers: a review of typical applications and studies on power draw, flow pattern, energy dissipation and transfer properties. Chem. Eng. Process: Process Intensif. 57, 25–41.
Zhang, Y., Zhang, Y., She, W., Yang, L., Liu, G., Yang, Y., 2019. Rheological and harden properties of the high-thixotropy 3D printing concrete. Construct. Build. Mater. 201, 278–285.
Zhi, P., Wu, Y.-C., Yang, Q., Kong, X., Xiao, J., 2022. Effect of spiral blade geometry on 3D-printed concrete rheological properties and extrudability using discrete event modeling. Autom. ConStruct. 137, 104199.